NANO LETTERS
Cite This: Nano Lett. XXXX, XXX, XXX−XXX
Letter
pubs.acs.org/NanoLett

Bacterial Nanobionics via 3D Printing

Sudeep Joshi, Ellexis Cook, and Manu S. Mannoor*

Neuro-Bionics and Neuro-Electric Medicine Laboratory, Department of Mechanical Engineering, Stevens Institute of Technology, Hoboken, New Jersey 07030, United States

Supporting Information

ABSTRACT: Investigating the multidimensional integration between different microbiological kingdoms possesses potential toward engineering next-generation bionic architectures. Bacterial and fungal kingdom exhibits mutual symbiosis that can offer advanced functionalities to these bionic architectures. Moreover, functional nanomaterials can serve as probing agents for accessing newer information from microbial organisms due to their dimensional similarities. In this article, a bionic mushroom was created by intertwining cyanobacterial cells with graphene nanoribbons (GNRs) onto the umbrella-shaped pileus of mushroom for photosynthetic bioelectricity generation. These seamlessly merged GNRs function as agents for mediating extracellular electron transport from cyanobacteria resulting in photocurrent generation. Additionally, three-dimensional (3D) printing technique was used to assemble cyanobacterial cells in anisotropic, densely packed geometry resulting in adequate cell-population density for efficient collective behavior. These 3D printed cyanobacterial colonies resulted in comparatively higher photocurrent (almost 8-fold increase) than isotropically casted cyanobacteria of similar seeding density. An insight of the proposed integration between cyanobacteria and mushroom derives remarkable advantage that arises from symbiotic relationship, termed here as engineered bionic symbiosis. Existence of this engineered bionic symbiosis was confirmed by UV−visible spectroscopy and standard plate counting method. Taken together, the present study augments scientific understanding of multidimensional integration between the living biological microworld and functional abiotic nanomaterials to establish newer dimensionalities toward advancement of bacterial nanobionics.

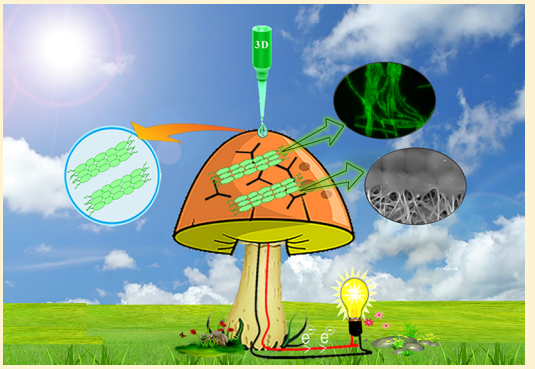

KEYWORDS: *Additive manufacturing, bionic symbiosis, cyanobacteria, graphene nanoribbons, mushroom, photosynthetic bioelectricity*

The covert biological microworld is comprised of a plethora of micro-organisms which holds astounding, yet untapped functionalities, that offer enormous opportunities for exploration. These microbial species coexist, efficiently interact, and perform incredible tasks to maintain self-sustaining microbiota. The biological microworld is classified into several kingdoms, wherein bacterial and fungal kingdoms reap mutual benefits by exhibiting significant mutualistic symbiosis.[1−3] Therein lies a greater engineering challenge in utilizing inherent capabilities and functionalities by selectively and controllably teaming-up different species from the biological microworld to realize functional bionic architectures toward innovative applications. Therefore, a compelling scientific interest is to pay attention for inquisitive resources and techniques for tapping into the biological microworld for better cognizance leading toward novel opportunities.

Bacterial cells in densely packed forced colonies perform phenomenal social activities for accomplishing complex functionalities such as, bioluminescence (exhibited by *Vibrio fischeri*[4]), transferring of genetic materials,[5] and antibiotic production.[6] These bacterial cells in densely packed forced colonies utilize numerous communication pathways such as, employing low molecular weight autoinducers and signaling oligopeptides,[7,8] packaging molecules into extracellular membrane vesicles,[9] and formation of channeling structures known as microplasmodesmata.[10] Likewise, intracellular channels facilitate the exchange of molecules and growth factors that results in mutually dependent metabolic activities for efficient functionalities.[11] There is a persuasive engineering challenge to avail this collective behavioral ability of bacteria resulting from cell-population density to create a functional bionic architecture.

Among the prolific bacterial species of scientific interests, cyanobacteria possess a unique ability for photosynthetic energy conversion with an unmatched internal quantum efficiency of nearly 100%.[12] The evolution of photosynthetic organisms over 2.5 billion years has resulted in the most efficient antenna systems for absorbing incident light energy and systematically directing it to reaction centers, followed by charge separation.[13] Thus, nature maps the most efficient way to utilize solar energy by converting it into chemical bonds during the process of photosynthesis performed by plants and

Received: June 28, 2018
Revised: October 11, 2018

DOI: 10.1021/acs.nanolett.8b02642
Nano Lett. XXXX, XXX, XXX−XXX

certain bacterial species. A soluble pigment−protein complex type of photosynthetic antennae, namely cyanobacterial Phycobilisomes, perform the function of harvesting light energy in cyanobacteria.[14] Micro-organisms that possess such photosynthetic capabilities embrace potential applications toward advancements in fields such as bacteriology,[15] energy harvesting,[16] genetic engineering,[17] and bacterial nanobionics. We propose to utilize this light energy conversion capability of cyanobacteria to realize a bionic architecture for photosynthetic bioelectricity generation studies.

To realize such a bionic architecture, nature provides inspiration from a few organisms that have evolved over millions of years and upholds the compelling structure for biomimicking. Mushroom is one such living organism that belongs to the fungi kingdom and classifies as saprophytes. Mushroom's pileus can be utilized resourcefully to immobilize densely packed forced cyanobacterial colonies for efficient photosynthetic bioelectricity generation. Water molecules required for photosynthesis can be delivered to immobilized cyanobacteria via capillary action of hydrophilic fibrous stripes called hyphae, which runs from the underground mycelium, toward the mushroom's pileus. Moreover, the mushroom's porous structure transfers water molecules within the pileus and hence provides the necessary water channels. Recently, these structural properties of the mushroom were effectively explored for efficient solar steam-generation devices.[18] We propose to harness these unique structural properties of the mushroom to realize a functional bionic mushroom, by interweaving cyanobacterial cells on its pileus. Engineering a multidimensional integration among different microbiological kingdoms can harness advantage by exploring the existence of rational bionic symbiosis. As the mushroom lacks the ability to perform photosynthesis[19] due to the absence of chlorophyll pigments, these seamlessly intertwined cyanobacterial colonies can impart photosynthesis functionality to the mushroom. Concurrently, the mushroom's structure provides self-serving biophysiological conditions, such as humid shelter and stable source of nutrients for cyanobacterial colonies to survive longer. Hence, the proposed integration derives mutual benefits and is termed as "engineered bionic symbiosis". We have performed a comparative study to explore the suitability of a biotic substrate (button mushroom) for long-time duration cyanobacterial survival as compared to commonly used biocompatible substrate (polysiloxane).

Likewise, the continually progressing field of functional abiotic nanomaterials possesses the potential to act as probing agents for accessing information to gain newer understandings of the biological microworld due to their dimensional similarities.[20] Tailoring materials at nanometer dimensions offers enhanced functionalities over their bulk counterparts.[21−23] These functional nanomaterials exhibit properties for wide-ranging applications such as antimicrobial resistance,[24] optoelectronics,[25] piezoelectricity,[26,27] superhydrophobic surfaces,[28] sensing,[29,30] actuation,[31] energy harvesting,[32] and storage.[33] Recent advancements in research efforts toward effective integration of functional abiotic nanomaterials, such as carbon nanotubes (CNTs)[16] and gold nanoprobes[34] with bacterial and algal cells demonstrates promising aspects. Therefore, we reason that the interaction between biological microworld with abiotic nanomaterials should be explored further to realize an advanced functional bionic mushroom structure.

In the present article, a bionic mushroom (Figure 1A) was created for photosynthetic bioelectricity generation using

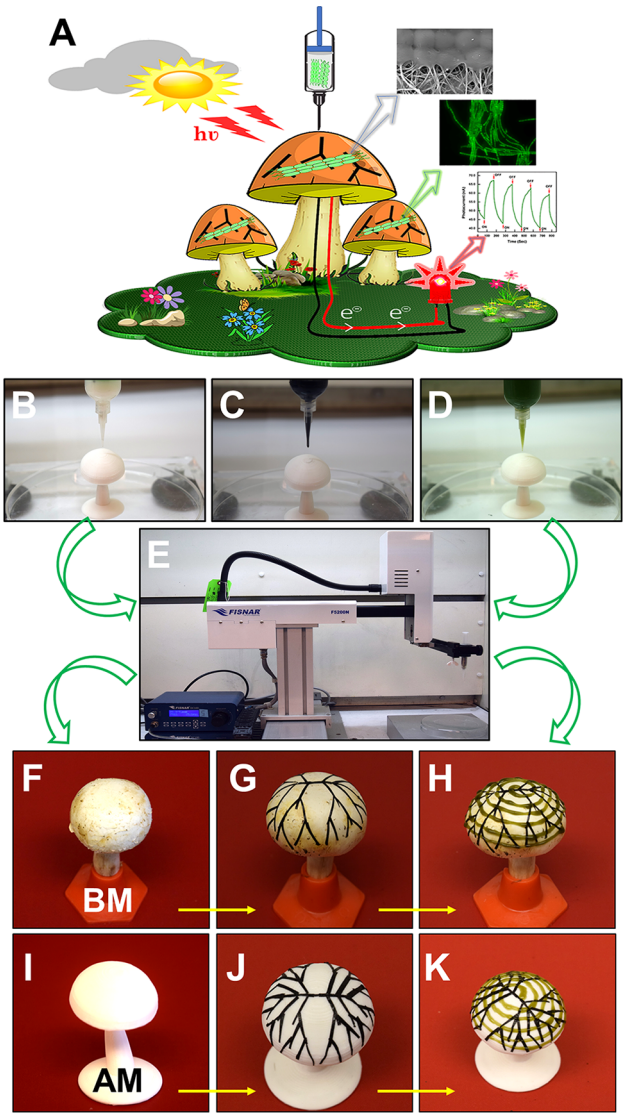

Figure 1. (A) A schematic of bionic mushroom with 3D printed cyanobacterial colonies for photosynthetic bioelectricity generation. (B) Polysiloxane as a structural scaffold support material. (C) GNRs uniformly dispersed in PEDOT:PSS conductive matrix as an electronic-ink for printing electrode network. (D) Cyanobacterial cell culture preseeded in alginate hydrogel matrix constituting biological-ink. (E) A robotic arm (Fisnar F5200N) modified as a pneumatic extrusion-based 3D printing machine. (F,I) Button mushroom (biotic mushroom, BM) and artificial mushroom (abiotic mushroom, AM). (G,J) Electrode network printed in Fibonacci sequence on BM and AM, and (H,K) 3D printed cyanobacterial colonies on BM and AM, respectively.

three-dimensional (3D) printing technique to generate densely packed anisotropic cyanobacterial (*Anabaena*) colonies seamlessly merged with abiotic nanomaterial (graphene nanoribbons, GNRs) onto the umbrella-shaped pileus. Recently, our group has successfully demonstrated the 3D interweaving of biological tissue with functional electronics for creating bionic ears.[35] Taking this a step further, this work explores 3D multimaterial printing for seamless intertwining of abiotic and biotic microworld. Previously, few attempts toward 3D

DOI: 10.1021/acs.nanolett.8b02642
Nano Lett. XXXX, XXX, XXX−XXX

printing of bacterial cells have shown promising applications for material production[36,37] and enhanced antibiotic resistance due to 3D arrangement.[38] We demonstrate a notable capability to utilize spatial and organizational ability of 3D printed cyanobacterial cells to realize a functional bionic mushroom for photosynthetic bioelectricity generation. Furthermore, we have accomplished direct 3D printing on a living mushroom by precisely considering the intricate gradients of its umbrella-shaped pileus. Additionally, a remarkable insight of the present integration arises from symbiotic relationship between cyanobacterial cells and mushroom, resulting in the longer life-span of cyanobacteria. The investigation of this engineered bionic symbiosis is confirmed by UV−visible spectroscopy and standard plate counting method.

A comparative study was undertaken for demonstrating photosynthetic bioelectricity generation from 3D printed and isotropically casted cyanobacterial cells immobilized on a biotic and abiotic mushroom. Figure 1B−E shows structural (polysiloxane), electronic (GNRs + PEDOT:PSS) and biological (cyanobacterial cells) materials fed into a pneumatically controlled syringe of a robotic arm (Fisnar F5200N) assembled to function as a 3D printer. A culinary button mushroom (as biotic mushroom, BM), and 3D printed polysiloxane structure (as abiotic mushroom, AM) were employed as substrates (Figure 1F,I). First, a highly conductive percolated network of GNRs[39] uniformly dispersed in PEDOT:PSS (poly(3, 4-ethylenedioxythiophene) polystyrene-sulfonate) solution, 2% (w/v) was constituted as electronic-ink to print the electrode network (see Experimental Methods). The conductivity of printed electronic-ink was 0.47 ± 0.02 S/cm as measured by four-point conductivity measurement. This was followed by bioink preparation using the protocol modified from our previous work.[35] In the present study, bioink is formulated by gently vortexing alginate hydrogel with an exponentially growing cyanobacterial cells in nutrient-rich medium (Alga-Gro by Carolina) at an optimized concentration of 4% (w/v) (see Supporting Information: preparation of printing inks). To evaluate the viscoelastic property of as-prepared electronic-ink and bioink, these inks were subjected to an increasing shear rate variation with a rotational rheometer (Figure S1A,B). The electronic-ink was tested in a shear ramp test running from 0.1 to 10 s^{-1} and bioink from 1 to 1000 s^{-1} shear rate over the duration of 2 min. Both these inks exhibited a noticeable shear thinning behavior typically encountered for uniformly dispersed suspensions,[40] hence facilitating the printing process with good reliability resulting from higher viscosity. These inks were efficiently printed with a needle size of 27G (inner diameter of 210 μm), as optimized during our previous work.[35] The as-prepared electronic-ink was printed in a Fibonacci series pattern on mushroom's pileus, an inspiration from natural biological structures.[41] This specific pattern was selected because it provides uniformly branched electrode network resulting in the maximum coverage of pileus surface area (Figure 1G,J). This was followed by bioink printing in spiral shape pattern on top of Fibonacci electrode network,[42] allowing for multitudinous cross-sectional contact areas between cyanobacterial cells and electrode network (Figure 1H,K). During the printing of bioink, ionic cross-linking of alginate was initiated by spraying $CaCl_2$ solution (0.25 M concentration in DI water) resulting in the structural stability of printed spiral bioink over mushroom's pileus. Altogether, the resulting structure is a 3D printed bionic mushroom seamlessly integrating biotic world (cyanobacterial cells and mushroom) with abiotic nanomaterials (GNRs + PEDOT:PSS) for photosynthetic bioelectricity generation.

Microscopic studies were conducted for investigating spatial alignment and distribution of cyanobacterial cells in 3D printed and isotropically casted samples (Figure 2). It is visibly evident that the 3D printed sample remarkably accomplished anisotropically aligned and densely packed cyanobacterial colonies, rather than isotropically casted sample for equal

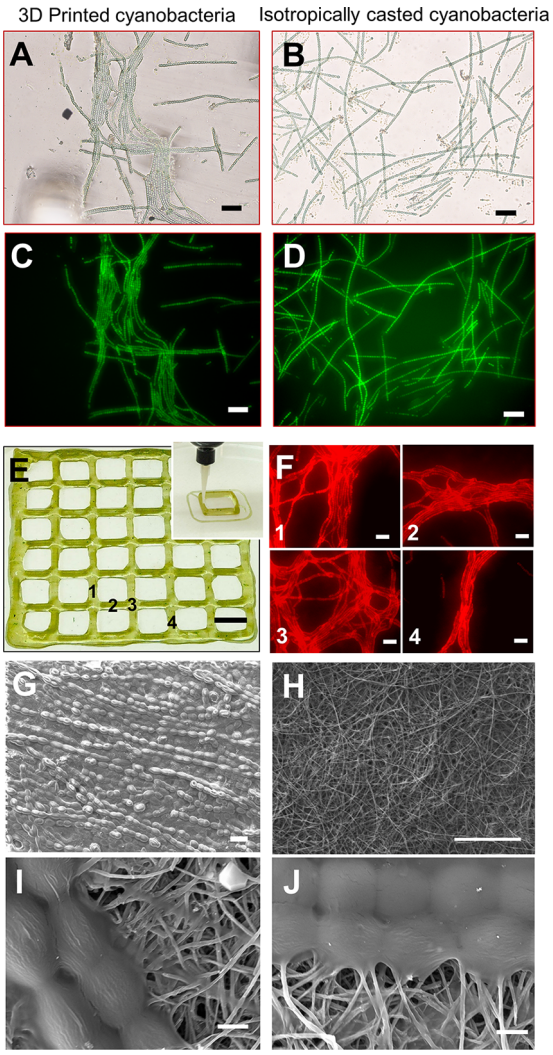

Figure 2. Microscopic studies. (A,B) Bright-field microscopic images showing anisotropically aligned densely packed 3D printed cyanobacterial colonies and isotropically casted randomly distributed cyanobacterial cells, respectively (scale bar: 50 μm). (C,D) Calcein dye fluorescence signals (scale bar: 50 μm). (E) The 3D printing of bioink in a square mesh structure (height in z-direction ∼7−8 mm) (scale bar: 1 cm). Inset: magnified view of a single unit block. (F) Strong autofluorescence signal emission from chlorophyll pigments of 3D printed cyanobacterial cells at four different locations (1−4 on square mesh) indicating anisotropically aligned cyanobacteria in the direction of printing path (scale bar: 20 μm). (G) SEM image showing morphological structure of 3D printed cyanobacteria depicting anisotropic and orderly alignment (scale bar: 20 μm). (H) Highly conductive percolated network of uniformly dispersed GNRs in PEDOT:PSS solution (electronic-ink) (scale bar: 10 μm). (I,J) Multitudinous direct physical attachment sites between GNRs and outer membrane of cyanobacterial cells at two different locations (scale bar: 2 μm).

DOI: 10.1021/acs.nanolett.8b02642
Nano Lett. XXXX, XXX, XXX−XXX

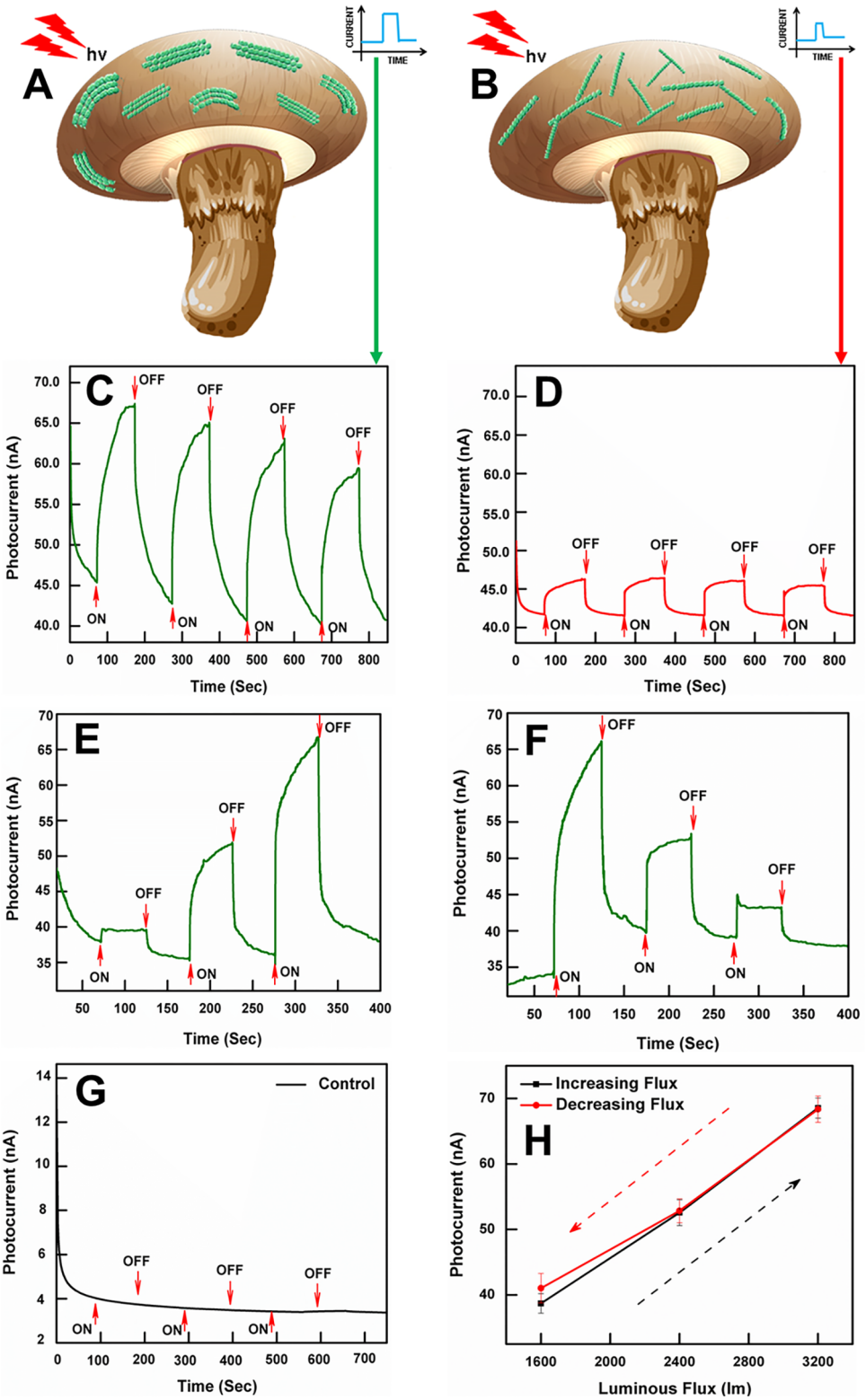

Figure 3. Photosynthetic bioelectricity generation studies. (A,B) Schematic representation of 3D printed and isotropically casted cyanobacteria on mushroom's pileus, respectively. (C,D) Amperometric studies ($i-t$ curves) over numerous light on/off cycles. (C) Photocurrent generation from 3D printed cyanobacteria shows an almost 8-fold increase in photocurrent. (D) Photocurrent generation from isotropically casted cyanobacteria. (E,F) Luminous flux variation studies generated a noteworthy mirror image pattern for photocurrent variation in 3D printed cyanobacteria sample: (E) lower to higher luminous flux variation and (F) higher to lower luminous flux variation. (G) Photocurrent response from control sample (free-standing films of GNRs + PEDOT:PSS) does not show detectable photocurrent during several light on/off cycles. (H) Variation of photocurrent amplitude versus luminous flux shows linear characteristic. (Increasing order of luminous flux (black) and decreasing order of luminous flux (red)) ($N = 5$).

DOI: 10.1021/acs.nanolett.8b02642
Nano Lett. XXXX, XXX, XXX−XXX

seeding density of cyanobacterial cell culture (4% w/v) (Figure 2A,B). Further, these samples were then loaded with a nonfluorescent acetoxymethylester (AM) derivative Calcein dye, that readily traverses cell membrane wherein ester groups are hydrolyzed by esterase to produce a fluorescent hydrophilic product.[43,44] Calcein dye was transported through the as-prepared bioink and effectively taken up by 3D printed cyanobacteria indicating highly porous matrix for effectively delivering Calcein to embedded cyanobacterial cells (Figure 2C,D). Moreover, to illustrate versatility of the as-prepared bioink, a square mesh pattern was also 3D printed (Figure 2E). Self-standing structures of about 7−8 mm height in *z*-direction (individual layer thickness of ∼0.8 to 1 mm) were printed (Figure 2E, inset). Four different locations (1−4) are indicated on the printed square mesh; corresponding autofluorescence emission from encapsulated cyanobacterial cells at these locations are displayed in Figure 2F. Noticeably, the cyanobacterial cells tends to significantly align in the direction of defined printing path leading toward direction-dependent anisotropic geometry. The observed induced anisotropy is the result of embedded cyanobacterial cells in bioink undergoing shear-induced alignment as they flow through the printing nozzle head.[45] The emission of autofluorescence from chlorophyll pigments located in thylakoid membranes of cyanobacteria, which are the site for light-dependent reactions during photosynthesis, indicates live and healthy cells entwined in bioink matrix after the printing process. This establishes our 3D printing technique to be cytocompatible allowing assemblage of cyanobacterial cells in anisotropic arrangement. Different structural geometries were printed during the optimization of bioink for printing purpose, wherein we have observed similar anisotropy of cyanobacterial cells in the direction of prescribed printing path (see Supporting Information, Figure S2A−F).

For observing and analyzing the interaction between cyanobacterial cells (embedded in bioink) and graphene nanoribbons (uniformly dispersed in electronic-ink), scanning electron microscopy (SEM) studies were performed by employing standard cell fixing protocol (see Experimental Methods). Figure 2G,H shows surface morphology of 3D printed cyanobacteria depicting anisotropic and orderly alignment and highly conductive percolated network of uniformly dispersed GNRs in PEDOT:PSS solution (electronic-ink), respectively. Further, analysis of SEM images reveals the presence of substantial voluminous direct physical attachment sites between GNRs and outer membrane of cyanobacterial cells (Figure 2I,J). These attachment sites act as pathways for direct transfer of extracellular electrons generated during photoinduced water oxidation reaction by facilitating efficient electron transfer through the outer membrane redox proteins.[16] Use of highly conductive ribbon-like functional nanomaterial for transferring of extracellular electrons is advantageous because these structures provide multitudinous points of contacts resulting in higher electron flux transfer. The amperometric response of cyanobacterial cells to alternate light and dark illumination cycles evidently demonstrates extracellular electron flux transfer facilitated through GNRs and is discussed in detail in the following section.

A few prior successful attempts had shown notable light-dependent electrogenic activity for different genetic variants of cyanobacteria.[16,46] Therefore, light-dependent photocurrent generation can serve as a suitable evaluation parameter for our experiments to compare performance characteristics of 3D printed and isotropically casted cyanobacterial cells on mushroom's pileus. Figure 3A,B illustrates the schematic representation of 3D printed and isotropically casted cyanobacterial cells on a biotic mushroom's pileus, wherein the same number of cyanobacterial cells (4% w/v) were used for comparing their photocurrent generation performance. The 3D printed Fibonacci electrode pattern on the mushroom's pileus serves as a working electrode, a platinum wire as a counter electrode, and Ag/AgCl as a reference electrode thus making the arrangement as a three-electrode setup. The working electrode was extended through the stem of biotic mushroom's structure for electrical connection purpose and the cross-sectional image is depicted in Figure S3 (see Supporting Information). The experiments were conducted on a biotic mushroom at an applied bias voltage of 0.5 V in 100 mM phosphate buffer saline with pH 7.4 used as the electrolyte solution. Photocurrent measurement experiments were performed under a photosynthetically active radiation (PAR) source, having variable luminous flux settings (Dolan Jenner, Fiber Lite). The effect of periodic light on/off cycle is notably established from the amperometric (current versus time, *i*−*t* curve) for both the 3D printed and isotropically casted cyanobacteria sample in Figure 3C,D. When illuminated with a light source, the photocurrent exhibited a sharp increase until reaching a plateau level, and a steep decrease as the light source is turned off. The source of electrons resulting in light-dependent photocurrent is the PS-II (photosystem II), wherein plastoquinone (PQ) plays a vital role of transporting electrons from photosynthetic electron transport chain (P-ETC) to extracellular environment.[46] Subsequently, these extracellular electrons were transferred via outer membrane redox proteins to the physically attached GNRs dispersed on the electrode surface. Further, it is also interesting to note that the 3D printed cyanobacterial sample recorded an almost 8-fold increase in photocurrent generation (Figure 3C), hence clearly outperforming the isotropically casted cyanobacterial sample of similar seeding density (Figure 3D) over numerous light and dark cycles. The probable reason for such a higher photocurrent is the ability of 3D printed sample to assemble cyanobacterial cells in densely packed geometry thus, facilitating physical connections resulting in molecular exchange and information-sharing via conjugation.[47] Moreover, the observed increase in photocurrent is also attributed to the ability of cyanobacterial cells in 3D printed forced colonies to have synergic communication resulting in synchronized collective behavioral characteristics, which is not possible for isotropically casted samples. Similar evidence demonstrating collective cell behavior due to confinement of *Pseudomonas aeruginosa* bacteria in small volumes and densely packed arrangement for initiating quorum sensing (QS) is observed by Boedicker et al.[48] Therefore, our efforts underlines a novel concept of using 3D printing to generate densely packed forced cyanobacterial colonies resulting in adequate population densities to operate in synergic manner for photocurrent generation.

The control sample employed in our present study was free-standing films of GNRs dispersed in PEDOT:PSS solution (acting as electrodes). Notably, light on/off experiments on control sample does not produce any detectable photocurrent during several light and dark cycles (Figure 3G). Additionally, we have conducted control experiments with dead cyanobacterial cells to support the claim of photocurrent generation resulting from the extracellular electron transport associated

DOI: 10.1021/acs.nanolett.8b02642
Nano Lett. XXXX, XXX, XXX−XXX

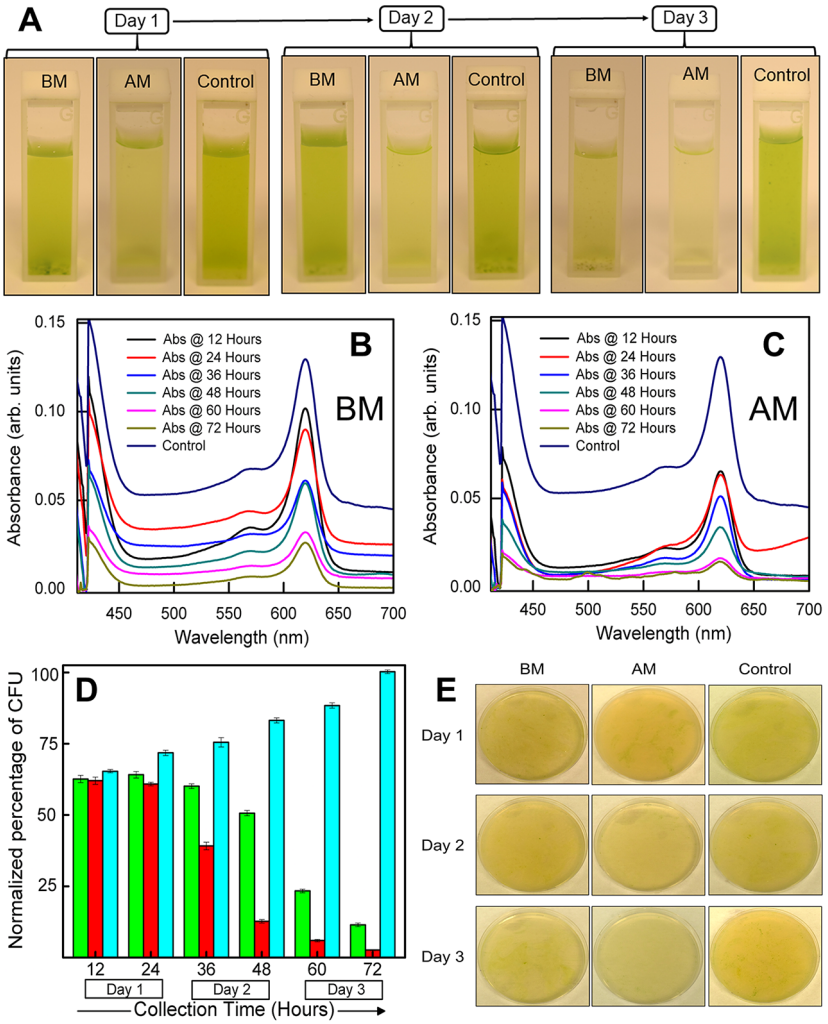

Figure 4. Engineered bionic symbiosis studies. (A) Photograph of samples showing an evident decrease in cyanobacterial cell density collected from BM and AM on three different days. (B,C) Absorbance spectra variation of (Chl-a) pigment extracted from cyanobacterial samples collected from BM and AM, respectively. (D) Variation of normalized percentage of Colony Forming Unit (CFU) with respect to cyanobacterial samples collected at different time intervals (T_c) from agar plate counting method ($N = 5$) (bar colors: green, samples collected from BM; red, samples collected from AM; blue, control samples). (E) Standard plate counting method showing agar plates for estimating cyanobacterial growth kinetics for different collection time (T_c) interval.

with cyanobacterial metabolism. To kill cyanobacterial cells, we have treated these cells with 100% methanol solution and have kept it in dark at 4 °C for the duration of 12 h. Figure S4 shows bright-field and fluorescence microscopic studies conducted to confirm cyanobacterial cell-death from methanol treatment. The cyanobacterial cells treated with 100% methanol solution emitted no red autofluorescence confirming cell death.[49] These dead cyanobacterial cells were then examined for photocurrent generation studies by maintaining all other parameters constant as for healthy/live cyanobacterial cells. As can be noted, light on/off experiments with dead cyanobacterial cell sample does not produce any detectable photocurrent during several light and dark cycles during experiment conducted for the duration of about 45 min (Figure S5). Therefore, the two control studies (Control 1, only PEDOT:PSS without cyanobacterial cells (Figure 3G), and Control 2, dead cyanobacterial cells (Figure S5)) support the claim of detected photocurrent generation from the extracellular electron transport associated with cyanobacterial cells during the light illumination studies in the presence of a photosynthetically active light source.

Additionally, we proceeded with experiments to examine the dependence of photocurrent amplitude on luminous flux variations for 3D printed cyanobacteria sample. This study establishes linearity, reproducibility, and repeatability of generated photocurrent in a single experimental run. Interestingly, the 3D printed cyanobacteria sample responded faithfully to the increasing (Figure 3E) and decreasing (Figure 3F) luminous flux variations over three light and dark cycles. It is evident from Figure 3E,F that luminous flux variation studies generated a noteworthy mirror image pattern for dependence of photocurrent on luminous flux. Moreover, the generated photocurrent follows almost linear variation trend for increasing and decreasing luminous flux (Figure 3H). The minimum amount of luminous flux required for 3D printed sample to generate a stable photocurrent (i.e., photocurrent reaching a plateau level) is about 1600 lm, whereas the maximum allowable luminous flux is about 3200 lm. Exposure of cyanobacterial cells above this luminous flux is detrimental to outer membrane proteins resulting in their denaturation and thus affecting the functioning of bionic mushroom.

DOI: 10.1021/acs.nanolett.8b02642
Nano Lett. XXXX, XXX, XXX−XXX

An interesting aspect of integrating cyanobacterial cells over mushroom's pileus originates from the existence of endosymbiotic relationship between bacterial cells and fungi offering numerous benefits.[50] In our present study, we have explored such an engineered bionic symbiosis contributing toward a novel functionality of enhanced life-span of cyanobacteria. The biotic mushroom's structure is rich in moisture content, provides suitable canopy, and, hence mimics appropriate biophysiological environment for supporting viable bacterial colonies. The following section describes experimental efforts to establish engineered bionic symbiosis, resulting in enhanced life-span of cyanobacterial cells immobilized on mushroom's pileus. Previous studies have shown label-free spectroscopy method based on optical density (OD) measurements using UV−visible spectroscopy as an effective technique to determine bacterial cell concentration in culture media.[51] Likewise in the present study, UV−visible spectroscopy was employed to determine pigment concentration from cyanobacterial cell suspension and, concurrently, a standard plate counting method was employed to examine cyanobacterial growth kinetics to support the claim of engineered bionic symbiosis.

The 3D printed cyanobacteria on pileus of both mushrooms' BM and AM, Figure 1H,K were incubated at an ambient temperature of ∼27 °C and were examined for enhanced life-span of cyanobacterial cells. Immobilized cyanobacteria samples from both mushroom's pileus were collected at regular intervals of 12 h (T_c) for 3 days duration. The periodically collected samples were then incubated in nutrient-rich medium (Alga-Gro by Carolina) (pH ∼ 7.8) and alongside seeded on agar plates for standard plate counting to determine viable cyanobacterial growth. Concurrently, samples were collected at similar time intervals (T_c = 12 h) from a freshly growing cyanobacteria culture and was incubated in nutrient-rich medium and seeded on agar plate as a control sample for the experiment. These cyanobacterial samples collected at different time intervals (T_c) were allowed to enter the exponential growth phase, as during this phase cell division proceeds at a constant rate.[51,52] These exponentially growing cyanobacterial samples were then collected for experiments that allowed a reasonable comparison between samples collected at different time intervals (T_c). Chlorophyll-a (Chl-a) is a major photosynthetic pigment present in cyanobacteria, which contributes largely toward photocurrent generation.[16] Therefore, the incubated cyanobacterial samples in nutrient-rich medium were collected and examined for Chl-a pigment concentrations with UV−visible spectroscopy (see Experimental Methods). Higher concentration of Chl-a pigment directly corresponds to a greater number of viable cyanobacterial cells, resulting in higher absorbance from the corresponding sample. Absorbance spectra for samples collected from both mushrooms (BM and AM) follows a steadily decreasing trend for longer collection time (T_c), indicating that a longer collection time leads to lesser viable cell density and, hence, reduced absorbance from extracted pigments (Figure 4B,C). Interestingly, cyanobacterial samples collected from BM (Figure 4B) shows relatively higher absorbance as compared to samples collected from AM (Figure 4C) for similar collection time (T_c). This observation indicates that biotic mushroom pileus supports cyanobacterial cell viability for longer time duration, as compared to the abiotic mushroom. The biotic mushroom's pileus is porous and possesses fibrous stripes which efficiently absorbs the nutrient-rich medium from the 3D printed bioink and hence acts as a reservoir of essential nutrients for cyanobacterial cell growth for longer time duration (see Supporting Information Figure S6). Moreover, biotic mushroom surface provides suitable temperature and pH for maintaining the viability of cyanobacterial cells. These supporting biophysiological conditions were absent for abiotic mushroom resulting in much lesser cyanobacterial cell viability for similar collection time (T_c).

Simultaneously, results from the standard plate counting method followed an exactly similar trend, wherein cyanobacterial cells collected during early hours resulted in greater number of isogenic colonies. As evident from Figure 4D, colony count significantly decreased for cyanobacterial samples collected from AM after 24 h (Day 1); however, for samples from BM the decreasing trend was observed after 48 h (Day 2). Figure 4E shows Agar plates used for counting cyanobacterial colonies indicating the difference in cyanobacterial growth for samples collected at different time intervals. Therein lies a strong corroboration between results observed with UV−visible spectroscopy and standard plate counting method, which paved the way for existence of engineered bionic symbiosis resulting in the increased life-span of cyanobacterial cells on biotic mushroom's pileus. Experiments were repeated five times during both methods resulting in better statistical claim for establishing the existence of an engineered bionic symbiosis.

Additionally, we have also conducted experimental studies to compare cyanobacterial cell viability on pileus of live and dead mushrooms to support the discussion on engineered bionic symbiosis (see Supporting Information Figures S7 and S8). Interestingly, this study also supports the claim of bionic symbiosis existence between cyanobacterial cells and live biotic mushroom. The pileus surface of live biotic mushroom absorbs nutrient-rich medium hence acts as a reservoir of essential nutrients for cyanobacterial cells to survive. Moreover, it provides suitable biophysiological conditions, such as pH (∼7.4) and temperature for cyanobacterial viability. The pileus of abiotic mushroom (polysiloxane) and dead mushroom (vinegar-killed) does not provide these suitable conditions resulting in short-time survival of cyanobacteria. Therefore, these two experimental studies establish the claim of engineered bionic symbiosis between live biotic mushroom and cyanobacterial cells.

In conclusion, our present experimental efforts establish 3D printing technique as an efficient method to generate densely packed, anisotropic cyanobacterial cells resulting in sufficient cell-population density for synergic operation, leading toward enhanced photocurrent generation. The rheological studies of as-prepared electronic-ink and bioink exhibited shear-thinning behavior indicating uniformly dispersed suspension and high viscosity resulting in better printability on mushroom's pileus. The seamless bionic intertwining of cyanobacterial cells with GNRs, provide effective pathways for direct extracellular electron transfer resulting in photocurrent during light illumination studies. Furthermore, an interesting dimensionality of engineered bionic symbiosis resulting from the present integration between cyanobacteria and mushroom was established from corroborating results from UV−visible spectroscopy and Agar plate counting method. Mushroom's pileus nurtures suitable biophysiological conditions (reservoir of nutrient-rich medium, apt temperature, pH condition, and moisture-rich environment) facilitating high-viability and

DOI: 10.1021/acs.nanolett.8b02642
Nano Lett. XXXX, XXX, XXX−XXX

enhanced life-span of cyanobacterial cells. Therefore, the presently developed 3D printed bionic mushroom architecture is an environment-friendly and green source of photosynthetic bioelectricity with advanced functionality of nourishing the energy producing cyanobacteria. We believe that techniques developed in the present research can also be extended to 3D print other bacterial colonies with smart hydrogel materials for advancing bionic integration studies. Moreover, we envisage that the 3D printing bacterial nanobionics approach can organize different bacterial species in complex arrangements to investigate spatial and environmental parameters for influencing other bacterial social behaviors, such as bioluminescence and virulence.

Experimental Methods. *Printing of Electrode Network.* Graphene nanoribbons (GNRs) (AZ EM Branchburg Plant) were procured and used in the present experimental study without any further modification. PEDOT:PSS of high conductivity grade as a thick consistent paste was obtained from Sigma-Aldrich. Different concentrations of GNRs in PEDOT: PSS solution, ranging from 1% to 2.5% w/v (with an interval of 0.5%) were tested to optimize a well-dispersed, percolated solution that resulted in long-range connectivity of graphene nanoribbon matrix by employing tip-ultrasonication at an ambient temperature for 30 min duration. The resulting as-prepared electronic-ink was a conformal and uniformly distributed solution (Figure 2H) used for 3D printing electrode network in a Fibonacci series pattern on the umbrella-shaped mushroom's pileus (Figure 1G,J).

SEM Sample Preparation. Samples were thoroughly rinsed with PBS buffer (pH ∼ 7.4) followed by dehydration in series of ethanol solutions (Sigma-Aldrich) at different concentrations (70%, 80%, 90%, and 100%) for 15 min duration. Later samples were dried with 2:1 solution of hexamethyldisilizane (HMDS) (Sigma-Aldrich) with ethanol for 15 min duration. In the final step, samples were then transferred to 100% HMDS inside a ventilated chemical fume hood and left for 12 h, allowing the HMDS to evaporate. The as-dried samples were then sputter-coated with ultrathin Au coating (thickness ∼5 nm) before loading them into the SEM (FESEM, Zeiss Auriga) chamber for imaging and analyzing the interaction between cyanobacterial cells and GNRs.

UV−visible Spectroscopy Studies. Exponentially growing samples of cyanobacterial suspension (2 mL) in nutrient-rich (Alga-Gro fresh water medium) were collected for these studies. These collected samples were centrifuged at 15 000×*g* for 10 min and the supernatant was discarded. Precooled (4 °C) methanol (0.5 mL) was added to cyanobacterial cell pellets and was homogenized by vortexing at 2800 rpm for 20 s duration. This was followed by incubating the samples at 4 °C in dark conditions for 30 min duration allowing for photosynthetic pigments to be extracted from cyanobacterial cells. The above solution is then centrifuged again at 15 000×*g* for 10 min duration to collect extracted pigments as pellets. In the final step, these samples were analyzed with UV−visible spectrophotometer (Cole-Parmer) with methanol as a reference sample. Samples were scanned from 400 to 700 nm with a slit width of 1 nm.

■ ASSOCIATED CONTENT

Supporting Information

The Supporting Information is available free of charge on the ACS Publications website at DOI: 10.1021/acs.nanolett.8b02642.

Culturing of cyanobacteria, preparation of printing inks, optimization of bioink concentration, photosynthetic bioelectricity generation, mushroom's structure pertinent for bioinspiration, and engineered bionic symbiosis studies with dead mushroom as a suitable control (PDF)

■ AUTHOR INFORMATION

Corresponding Author

*E-mail: mmannoor@stevens.edu.

ORCID

Manu S. Mannoor: 0000-0002-0493-2230

Author Contributions

S.J. conceived and designed the experiments. S.J. performed the experiments. E.C. performed SEM experiments and analysis. S.J. and M.S.M. wrote the manuscript. All authors have given approval to the final version of the manuscript.

Notes

The authors declare no competing financial interest.

■ ACKNOWLEDGMENTS

Authors gratefully acknowledge scanning electron microscopy (SEM) facilities provided by LMSI (Laboratory for Multi Scale Imaging) and UV−visible Spectroscopy facility at Prof. Attygalle Laboratory (Biomedical Engineering, Chemistry and Biological Sciences) at Stevens Institute of Technology, Hoboken, NJ, U.S.A.

■ ABBREVIATIONS

BM, biotic mushroom; AM, abiotic mushroom; GNRs, graphene nanoribbons; OD, optical density; CFU, colony forming units; PAR, photosynthetically active radiation

■ REFERENCES

(1) Ané, J.-M.; Kiss, G. B.; Riely, B. K.; Penmetsa, R. V.; Oldroyd, G. E. D.; Ayax, C.; Lévy, J.; Debellé, F.; Baek, J.-M.; Kalo, P.; Rosenberg, C.; Roe, B. A.; Long, S. R.; Dénarié, J.; Cook, D. R. *Science* **2004**, *303* (5662), 1364−1367.

(2) Henskens, F. L.; Green, T. G.; Wilkins, A. *Ann. Bot.* **2012**, *110* (3), 555−63.

(3) Büdel, B.; Scheidegger, C. Thallus morphology and anatomy. In *Lichen Biology*, 2nd ed.; Nash, I. I. I. T. H., Ed.; Cambridge University Press: Cambridge, 2008; pp 40−68.

(4) Nealson, K. H.; Platt, T.; Hastings, J. W. *Journal of bacteriology* **1970**, *104* (1), 313−322.

(5) Juhas, M.; van der Meer, J. R.; Gaillard, M.; Harding, R. M.; Hood, D. W.; Crook, D. W. *FEMS Microbiol Rev.* **2009**, *33* (2), 376−93.

(6) Bassler, B. L.; Losick, R. *Cell* **2006**, *125* (2), 237−46.

(7) Fuqua, C.; Greenberg, E. P. *Nat. Rev. Mol. Cell Biol.* **2002**, *3* (9), 685−95.

(8) Lazazzera, B. A. *Peptides* **2001**, *22* (10), 1519−27.

(9) Mashburn-Warren, L. M.; Whiteley, M. *Mol. Microbiol.* **2006**, *61* (4), 839−46.

(10) Giddings, T. H.; Staehelin, L. A. *Arch. Microbiol.* **1981**, *129* (4), 295−298.

(11) Golden, J. W.; Yoon, H. S. *Curr. Opin. Microbiol.* **2003**, *6* (6), 557−63.

(12) Blankenship, R. E.; Tiede, D. M.; Barber, J.; Brudvig, G. W.; Fleming, G.; Ghirardi, M.; Gunner, M. R.; Junge, W.; Kramer, D. M.; Melis, A.; Moore, T. A.; Moser, C. C.; Nocera, D. G.; Nozik, A. J.; Ort, D. R.; Parson, W. W.; Prince, R. C.; Sayre, R. T. *Science* **2011**, *332* (6031), 805−9.

(13) McConnell, I.; Li, G.; Brudvig, G. W. *Chem. Biol.* **2010**, *17* (5), 434−47.

DOI: 10.1021/acs.nanolett.8b02642
Nano Lett. XXXX, XXX, XXX−XXX

(14) Adir, N. *Photosynth. Res.* **2005**, *85* (1), 15−32.
(15) Flores, E.; Herrero, A. *Nat. Rev. Microbiol.* **2010**, *8* (1), 39−50.
(16) Sekar, N.; Umasankar, Y.; Ramasamy, R. P. *Phys. Chem. Chem. Phys.* **2014**, *16* (17), 7862−71.
(17) Sekar, N.; Jain, R.; Yan, Y.; Ramasamy, R. P. *Biotechnol. Bioeng.* **2016**, *113* (3), 675−9.
(18) Xu, N.; Hu, X.; Xu, W.; Li, X.; Zhou, L.; Zhu, S.; Zhu, J. *Adv. Mater.* **2017**, *29* (28), 1606762.
(19) Miles, P. G.; Chang, S.-T. *Mushroom Biology Concise Basics and Current Developments*; World Scientific: Singapore, 1997.
(20) Wong, M. H.; Giraldo, J. P.; Kwak, S.-Y.; Koman, V. B.; Sinclair, R.; Lew, T. T. S.; Bisker, G.; Liu, P.; Strano, M. S. *Nat. Mater.* **2017**, *16*, 264.
(21) Eustis, S.; El-Sayed, M. A. *Chem. Soc. Rev.* **2006**, *35* (3), 209−217.
(22) Joshi, S.; Nayak, M. M.; Rajanna, K. *ACS Appl. Mater. Interfaces* **2014**, *6* (10), 7108−16.
(23) Joshi, S.; Nayak, M. M.; Rajanna, K. *Small* **2018**, *14* (29), 1800608.
(24) Liu, C.; Kong, D.; Hsu, P.-C.; Yuan, H.; Lee, H.-W.; Liu, Y.; Wang, H.; Wang, S.; Yan, K.; Lin, D.; Maraccini, P. A.; Parker, K. M.; Boehm, A. B.; Cui, Y. *Nat. Nanotechnol.* **2016**, *11*, 1098.
(25) Ross, J. S.; Rivera, P.; Schaibley, J.; Lee-Wong, E.; Yu, H.; Taniguchi, T.; Watanabe, K.; Yan, J.; Mandrus, D.; Cobden, D.; Yao, W.; Xu, X. *Nano Lett.* **2017**, *17* (2), 638−643.
(26) Joshi, S.; Hegde, G. M.; Nayak, M. M.; Rajanna, K. *Sens. Actuators, A* **2013**, *199*, 272−282.
(27) Joshi, S.; Parmar, M.; Rajanna, K. *Sens. Actuators, A* **2012**, *187*, 194−200.
(28) Zhai, L.; Berg, M. C.; Cebeci, F. Ç.; Kim, Y.; Milwid, J. M.; Rubner, M. F.; Cohen, R. E. *Nano Lett.* **2006**, *6* (6), 1213−1217.
(29) Joshi, S.; Nayak, M. M.; Rajanna, K. *Appl. Surf. Sci.* **2014**, *296*, 169−176.
(30) Joshi, S.; Nayak, M. M.; Rajanna, K. In *Distributed piezoelectric Thin Film Sensor Array for monitoring impact events, 2013*; IEEE SENSORS: Baltimore, MD, USA, Nov. 3−6, 2013; pp 1−4, https://ieeexplore.ieee.org/abstract/document/6688459.
(31) Joshi, S.; Nayak, M. M.; Rajanna, K. In *Flexible phynox alloy with integrated piezoelectric thin film for micro actuation application, 2012*; IEEE Sensors: Taipei, Taiwan, Oct. 28−31, 2012; pp 1−4, https://ieeexplore.ieee.org/abstract/document/6411523
(32) Gaddam, V.; Joshi, S.; Parmar, M.; Rajanna, K.; Nayak, M. M. In *A novel piezoelectric ZnO nanogenerator on flexible metal alloy substrate, 2012*; IEEE Sensors: Taipei, Taiwan, Oct. 28−31, 2012; pp 1−4, https://ieeexplore.ieee.org/abstract/document/6411535.
(33) Frey, N. A.; Peng, S.; Cheng, K.; Sun, S. *Chem. Soc. Rev.* **2009**, *38* (9), 2532−2542.
(34) Ryu, W.; Bai, S.-J.; Park, J. S.; Huang, Z.; Moseley, J.; Fabian, T.; Fasching, R. J.; Grossman, A. R.; Prinz, F. B. *Nano Lett.* **2010**, *10* (4), 1137−1143.
(35) Mannoor, M. S.; Jiang, Z.; James, T.; Kong, Y. L.; Malatesta, K. A.; Soboyejo, W. O.; Verma, N.; Gracias, D. H.; McAlpine, M. C. *Nano Lett.* **2013**, *13* (6), 2634−2639.
(36) Schaffner, M.; Rühs, P. A.; Coulter, F.; Kilcher, S.; Studart, A. R. *Science Advances* **2017**, *3* (12), eaao6804.
(37) Lehner, B. A. E.; Schmieden, D. T.; Meyer, A. S. *ACS Synth. Biol.* **2017**, *6* (7), 1124−1130.
(38) Connell, J. L.; Ritschdorff, E. T.; Whiteley, M.; Shear, J. B. *Proc. Natl. Acad. Sci. U. S. A.* **2013**, *110* (46), 18380−5.
(39) Hu, L.; Kim, H. S.; Lee, J.-Y.; Peumans, P.; Cui, Y. *ACS Nano* **2010**, *4* (5), 2955−2963.
(40) Weis, C.; Oelschlaeger, C.; Dijkstra, D.; Ranft, M.; Willenbacher, N. *Sci. Rep.* **2016**, *6*, 33498.
(41) Li, C.; Zhang, X.; Cao, Z. *Science* **2005**, *309* (5736), 909.
(42) Ursyn, A. *Biologically-Inspired Computing for the Arts: Scientific Data through Graphics*; IGI Publishing: Hershey, PA, 2012.
(43) Mullineaux, C. W.; Mariscal, V.; Nenninger, A.; Khanum, H.; Herrero, A.; Flores, E.; Adams, D. G. *EMBO J.* **2008**, *27* (9), 1299−1308.
(44) Haugland, R. P. *Invitrogen: The Handbook; A Guide to Fluorescent Probes and Labeling Technologies*; Invitrogen Corp.: Carlsbad, CA, 2005.
(45) Gladman, A. S.; Matsumoto, E. A.; Nuzzo, R. G.; Mahadevan, L.; Lewis, J. A. *Nat. Mater.* **2016**, *15* (4), 413−8.
(46) Pisciotta, J. M.; Zou, Y.; Baskakov, I. V. *PLoS One* **2010**, *5* (5), e10821.
(47) Lederberg, J.; Tatum, E. L. *Nature* **1946**, *158* (4016), 558.
(48) Boedicker, J. Q.; Vincent, M. E.; Ismagilov, R. F. *Angew. Chem., Int. Ed.* **2009**, *48* (32), 5908−11.
(49) Liu, B. R.; Huang, Y.-W.; Lee, H.-J. *BMC Microbiol.* **2013**, *13* (1), 57.
(50) Artursson, V.; Finlay, R. D.; Jansson, J. K. *Environ. Microbiol.* **2006**, *8* (1), 1−10.
(51) McBirney, S. E.; Trinh, K.; Wong-Beringer, A.; Armani, A. M. *Biomed. Opt. Express* **2016**, *7* (10), 4034−4042.
(52) Sinetova, M. A.; Cerveny, J.; Zavrel, T.; Nedbal, L. *J. Biotechnol.* **2012**, *162* (1), 148−55.

DOI: 10.1021/acs.nanolett.8b02642
Nano Lett. XXXX, XXX, XXX−XXX